N84-26011

A sensitive optical pyrometer for shock-temperature measurements

Mark B. Boslough and Thomas J. Ahrens*

Seismological Laboratory

California Institute of Technology

Pasadena, CA 91125

ABSTRACT

A new optical system has been used to determine temperatures above 2400 K in shocked materials by measuring the spectral radiance of sub-microsecond pulses of light emitted from initially transparent solid samples in the visible and near-infrared (450-900 nm). The high sensitivity of this optical pyrometer can be attributed to the small number of channels (4), large aperture (0.03 steradian), the large bandwidth per channel (40 nm), and large photodiode detection area (0.2 cm^2). Improved calibration techniques reduce systematic errors encountered in previous shock-temperature experiments.

*present address: Sandia National Laboratories, Division 1131, Albuquerque, NM 87185

Introduction

Shock temperature measurements of initially transparent solids and fluids provide important constraints to the thermal equation of state of media at high shock pressures[1-10]. The present apparatus was designed to be used with a 2-stage light-gas gun, which launches 25 mm diameter projectiles that impact at speeds of 4 to 7 km/s against specimen assemblies. Shock pressures in the 50 to 200 GPa range are generated during the propagation time of the shock wave through the sample.

The present system was designed to be more sensitive to spectral radiance (and therefore to lower temperatures) than the previous narrow-band pyrometer described by Lyzenga and Ahrens.[3] This was achieved by trading off some spectral- and time-resolution for increased bandwidth and areal extent of the region of the shocked sample which is imaged onto the detector. The new system is over two orders of magnitude more sensitive in spectral radiance than the previous narrow-band pyrometer, and can be used to measure temperatures lower than 2500 K without preamplification of the signals. Fortunately, the loss of spectral- and temporal-resolution appears to be negligible in terms of data quality. Sensitivity might, in fact, be further increased by using even wider-band filters.

Experiment Design

The description of the optical pyrometer will proceed in the direction of light propagation, beginning with the target assembly (Figs. 1-2). Samples are typically transparent solids about 17 mm in lateral dimension and about 3 mm thick. Both surfaces are lapped to optical quality, and the samples are glued to flat metallic driver plates with epoxy. Great care is taken to minimize the gap between driver plate and target, and it is generally on the order of one micron

according to measurements made by counting visible fringes with an optical flat. In some cases the contact surface of the sample is aluminized before attaching it to the driver plate in order to mask any flash which might occur when the shock wave transits the gap.

The driver plates are circular disks 35 mm in diameter and 2 mm thick. The impact of the projectile against shorting pins protruding through holes in the driver plate generates a pulse for triggering the oscilloscope array some 200 ns before impact. The two pins, biased at 335 v, are mounted on the driver plate 9 mm above and below its center point, to avoid obscuring the light path.

It is necessary that the sample edges be masked because the field of view of the pyrometer is greater than the diameter of the sample. Edge effects (two-dimensional flow) occurs at only the outer portions of the sample. For this reason an aluminum edge-mask (painted black) is attached to the free surface of the sample. The mask contains a central 6 mm hole which provides the only path for the light signal from the sample to enter the pyrometer. The edge mask also supports 1 mm-diameter acrylic optical fibers, which carry light signals to an image converter streak camera, allowing simultaneous measurements of shock velocity and hence a pressure-density Hugoniot state[11].

The light generated in the sample is reflected by an aluminized mirror, turning it 90° toward the optical pyrometer port. The port through which the light is reflected is covered with a protective glass window which separates the evacuated target chamber from the objective lenses. The objective consists of two sets of achromats, with focal lengths of 50 cm and clear apertures of 11 cm. The target is near the focal point of the first achromat.

The converging light is separated into four legs by three beamsplitters (Fig. 3). The primary beamsplitter is an Ealing 22-8924 pellicle (stretched-membrane). The secondary beamsplitters are identical Melles-Griot 03 BTF 007

silvered plate-glass beamsplitters. Each of the four resulting beams falls upon a detector assembly. These consist of an interference filter, a focusing lens, and a silicon photodiode with a bias circuit (Fig. 4). The bandpass filters are 25.4 mm in diameter and have peak wavelengths in the visible or near infrared within the effective bandwidth range of the silicon photodiodes, between 400 and 1100 nm. Most of the filters we used have half-height bandwidths of about 40 nm.

Each channel utilizes an RCA C30822 N-type silicon pin photodiode, with an active area of .20 cm^2. In order to ensure that the image of the sample (and calibration lamp filament, which is larger) falls entirely within the photodiode active area, an 18 mm diameter, 15 mm focal length focusing lens was positioned between the filter and photodiode. This demagnifies the image by a factor of about 0.2. The detector assembly is mounted on a three-dimensional translation stage to allow alignment and focus adjustment. The focusing lens and filter holder can be moved independently to permit separate adjustment of focus and demagnification.

This optical configuration ensures that each detector views precisely the same image, only at a different wavelength. Thus, if the radiation is heterogeneously emitted, as would be the case if shear bands or hot spots developed[12,13], the average brightness would be measured by each detector. This eliminates the possibility of one detector viewing a hot spot while another views between hot spots. Also, by viewing the entire unmasked portion of the target, the sensitivity of the instrument is maximized (Fig. 5). Because the image is demagnified there is sufficient leeway in alignment and focusing, as long as the entire image falls on the active area of the detector.

The photodiode circuit is shown schematically in Fig. 4. The circuit supplies 45 V reverse bias from a battery to the photodiode. The signal is carried to oscilloscopes by a 50 Ω coaxial cable, where it is terminated by 50 Ω. The principal

recording oscilloscopes are Tektronix 485 models using series C-30 cameras with ASA 20,000 Polaroid type 612 film. The light gas gun on which these experiments are carried out is described by Jeanloz and Ahrens[14].

Calibration Procedure

A standard of spectral irradiance is placed in the position of the target in the impact chamber and the pyrometer is aligned. Spectral irradiance is the power radiated per unit wavelength per unit solid angle, regardless of the surface area of the radiator. The standard source used is a G.E. type Q6.6A/T4Q/1CL 200 watt tungsten-filament quartz-halogen lamp calibrated by Optronics Laboratories, Inc. The lamp is mounted on a target assembly and aligned in the same manner as a real target. It is driven by 6.50 Amperes from a Hewlett-Packard Model 6268B DC power supply constant current power supply. Current is monitored by a Keithley Model 173 digital multimeter, which measures the voltage across a .005 Ω resister in series with the lamp. The light beam incident on the pyrometer is physically chopped at about 200 Hz, and the resulting square wave is recorded. The voltage amplitude of the square wave, as recorded on each channel, is divided by the spectral irradiance of the lamp at the wavelength at which it is filtered. The resulting calibration factor is multiplied by the amplitude of the shock record to get the spectral irradiance of the shocked material. To determine the spectral radiance from which the temperature is calculated, the spectral irradiance is divided by the area of the hole in the edge mask. The solid angle need not be known, as long as the calibration lamp and the target are in the same position. This procedure is carried out prior to every shot, to account for differences between the expendable components (the mirror and window).

Because of the large (40 nm) half-height bandwidths of the filters used with this pyrometer, it is necessary to calculate the effective central wavelength of each filter, which is dependent on the spectral dependence of the other optical components, and on the temperature of the source. The other optical components have a weak spectral dependence relative to the filters, and this does not change greatly from shot to shot as components are replaced. It is thus possible to use nominal values published in component specifications, and measured values for the expendable components (the mirror and window) without greatly affecting the results. The wavelength-dependent parameters of the various optical components (Fig. 6) are defined in Table 1. All are measured with respect to λ, the wavelength in vacuum. The response of the 900 nm filter, for example, is shown in Fig. 8.

The spectral reduction factor of each channel, $r_i(\lambda)$ is given by:

$$r_1(\lambda) = R_M T_W T_L^2 T_{B_1} T_{B_2} T_1 T_1 R_d \tag{1}$$

$$r_2(\lambda) = R_M T_W T_L^2 R_{B_1} R_{B_2} T_1 T_2 R_d \tag{2}$$

$$r_3(\lambda) = R_M T_W T_L^2 T_{B_1} R_{B_2} T_1 T_3 R_d \tag{3}$$

$$r_4(\lambda) = R_M T_W T_L^2 R_{B_1} T_{B_2} T_1 T_4 R_d \tag{4}$$

The mean wavelength of channel i is therefore

$$\bar{\lambda}_i = \frac{\int_0^\infty r_i(\lambda)\lambda d\lambda}{\int_0^\infty r_i(\lambda) d\lambda} \tag{5}$$

There will also be a shift in effective wavelength as a function of temperature of the source, and this should be included. To calculate the shift, we must

assume *a priori* that the source radiates a Planck function.

The mean effective wavelength as a function of temperature is

$$\bar{\lambda}_i = \frac{\int_0^\infty r_i(\lambda) f(T,\lambda) \lambda d\lambda}{\int_0^\infty r_i(\lambda) f(T,\lambda) d\lambda}, \qquad (6)$$

where $f(T,\lambda)$ is the Planck function

$$f(T,\lambda) \quad \lambda^{-5}(e^{\frac{hc}{k_b \lambda T}} - 1)^{-1}. \qquad (7)$$

Where h, c, and k_b are Plancks constant, the speed of light and Boltzmans constant, respectively. The mean effective wavelengths for some of the channel-filter combinations which have been used are plotted in Fig. 7. A typical interference filter absorbance curve is shown in Fig. 8. The calibration lamp temperature is about 2700 K, so the effective wavelengths for calibration are those at 2700 K. The appropriate spectral irradiance is found by interpolating between values given by a table supplied by Optronics for the quartz halogen lamp[15].

Results and Conclusions

Spectral data from the two shock experiments carried out at shock pressures 48.3±2.2 and 84.5±1.3 GPa for a sample $CaAl_2Si_2O_8$ glass[10] are shown in Fig. 9. There were many different time dependences of radiance seen with the previous[3] and present systems. It is therefore difficult to compare results for different materials (Boslough, 1984, unpublished manuscript). Radiance versus time records were read at a specific point (just before shock arrival at the free surface). The sources of uncertainty arise from electrical noise, uncertainty in oscilloscope baseline, uncertainty in exactly the shock arrival at free-surface as well as errors in calibration.

The temperatures shown in Fig. 9 are obtained by assuming the shocked sample material radiates as a blackbody. If the emissivity, ε, as well as the temperature is allowed to vary upon inverting the radiance data for temperature, the resultant temperature varies by up to 150 K in the case of 2481 K experiment, and by only 8 K for the 4010 K experiment. Since unconstrained fits yield values of ε both above and below $\varepsilon = 1.0$, we assume these are not experimentally significant and thus assume $\varepsilon = 1.0$ is physically plausible. It should, however, be pointed out that a good physical model for the actual thermal radiation mechanism for a perfect radiator has not yet been proffered[18].

The present pyrometer achieved greater sensitivity and can reliably measure shock temperature down to temperatures as low as 2400 K, some 900 K lower than previously obtained, using photodiode detectors[3]. The present system achieves greater sensitivity on account of the use of a larger portion of the entire spectral, spatial, and angular output of the sample. This is because we record radiation into 0.03 steradian using four 40 nm bandwidth filters versus six 9 nm bandwidth filters of the earlier apparatus[3]. Additionally, the present system utilizes large area (0.2 cm^2) photodiodes onto which the image of the entire radiating portion of the sample is projected.

Acknowledgments: Research supported under NASA Grant NGL-05-002-105 and NSF-EAR81-16026. We are grateful for technical advice and assistance proffered by G. A. Lyzenga (JPL), E. Gelle, M. Long, and W. Ginn (Caltech), and R. J. Trainor (while at Lawrence Livermore National Laboratory) and the helpful use of Professor George Rossman's spectroscopy laboratory at Caltech. Division of Geological and Planetary Science contribution number 4073.

Figure Captions

Fig. 1. Photograph of shock-temperature target assembly from direction of pyrometer. Aperture (6.35 mm diameter) in edge mask can be seen in reflection in turning mirror. Optical fibers carry light pulse to streak camera.

Fig. 2. Configuration of shock-temperature experiments in which Hugoniot data are also obtained.

Fig. 3. Schematic of shock temperature-equation of state experiment.

Fig. 4. Circuit diagram for single optical pyrometer channel.

Fig. 5. Diagram showing approximate sensitivity range of optical pyrometer. Curves give spectral radiance as a function of wavelength for a 6.35 mm diameter blackbody emitter at the position of the target. Dashed lines represent wavelength of detectors in typical experiment. Unstippled area is within sensitivity range of silicon photodiodes.

Fig. 6. Schematic of optical pyrometer. Symbols are explained in Table 1.

Fig. 7. Mean effective wavelength $\bar{\lambda}$ of four wavelength-channel combinations, normalized to nominal filter wavelength λ_o.

Fig. 8. Absorbance versus wavelength for nominal 900 nm, 40 nm bandwidth, interference filter.

Fig. 9. Shock-induced radiance versus wavelength from two experiments at shock pressures of 48 and 84 GPa for $CaAl_2Si_2O_8$ glass[10].

References

[1] S. B. Kormer, M. V Sinitsyn, G. A. Kirillov, and V. D. Urlin, Sov. Phys. JETP 21, 689 (1965).

[2] S. B. Kormer, Sov. Phys. Usp. 11, 229 (1968).

[3] G. A. Lyzenga and T. J. Ahrens, Rev. Sci. Instrum. 50, 1421 (1979).

[4] G. A. Lyzenga and T. J. Ahrens, Geophys. Res. Lett., 7, 141 (1980).

[5] G. A. Lyzenga, T. J. Ahrens, W. J. Nellis, and A. C. Mitchell, J. Chem. Phys., 76, 6282 (1982).

[6] T. J. Ahrens, G. A. Lyzenga, and A. C. Mitchell, in High-Pressure Research in Geophysics, edited by S. Akimoto and M. H. Manghnani (Academic, Tokyo, 1982), p. 579.

[7] G. A. Lyzenga, T. J. Ahrens, and A. C. Mitchell, J. Geophys. Res., 68, 2319 (1983).

[8] W. J. Nellis, F. H. Ree, R. J. Trainor, A. C. Mitchell, and M. B. Boslough, J. Chem. Phys., 80, 2789 (1984).

[9] M. B. Boslough, T. J. Ahrens, and A. C. Mitchell, J. Geophys. Res. (submitted).

[10] M. B. Boslough, T. J. Ahrens, and A. C. Mitchell, Geophys. J. R. astr. Soc. (submitted).

[11] M. B. Boslough, S. M. Rigden, and T. J. Ahrens, Geophys. J. R. astr. Soc. (submitted).

[12] D. E. Grady, J. Geophys. Res., 85, 913 (1980).

[13] K. Kondo and T. J. Ahrens, Phys. Chem. Minerals, 9, 178 (1980).

[14] R. Jeanloz and T. J. Ahrens, in High Pressure Research, edited by M. H. Manghnani and S. Akimoto (Academic, New York, 1977), p. 439.

[15] M. B. Boslough, Ph.D. Thesis, California Institute of Technology, 1983, 171 pp.

[16] G. A. Lyzenga, in Shock Waves in Condensed Matter, edited by W. J. Nellis, L. Seamen, and R. A. Graham (Am. Inst. Phys., 1982), p. 268.

Table 1. Properties of Optical Components

Parameter	Definition	Source of Components	Source of Calibration
R_M	reflectance aluminized glass mirror	C & H Surplus Pasadena, CA	Lawrence Livermore National Laboratory, Standards Laboratory
T_W	transmittance plate glass port	Crown Glass Co. Pasadena, CA	Cary 17 spectrophotometer, Caltech
T_L	transmittance objective lens	Jaegers 35B1542	"
T_{B_1}	transmittance pellicle beamsplitter	Ealing 22-8924	Ealing Optics catalog
R_{B_1}	reflectance pellicle beamsplitter	Ealing 22-8924	"
T_{B_2}	transmittance plate-type beamsplitter	Melles-Griot 03BTF007	Melles-Griot Optics catalog
R_{B_2}	reflectance plate-type beamsplitter	Melles-Griot 03BTF007	"
T_l	transmittance of aspheric forming lens	Melles-Griot 01LAG003	Cary 17 spectrophotometer, Caltech
T_1, T_2, T_3, T_4	transmittance of broad-bandwith filter (40 nm)	Ealing Corp.	Cary 17 spectro-photometer, Caltech
R_d	responsivity of photodetector	RCA C30822	RCA specification sheet.

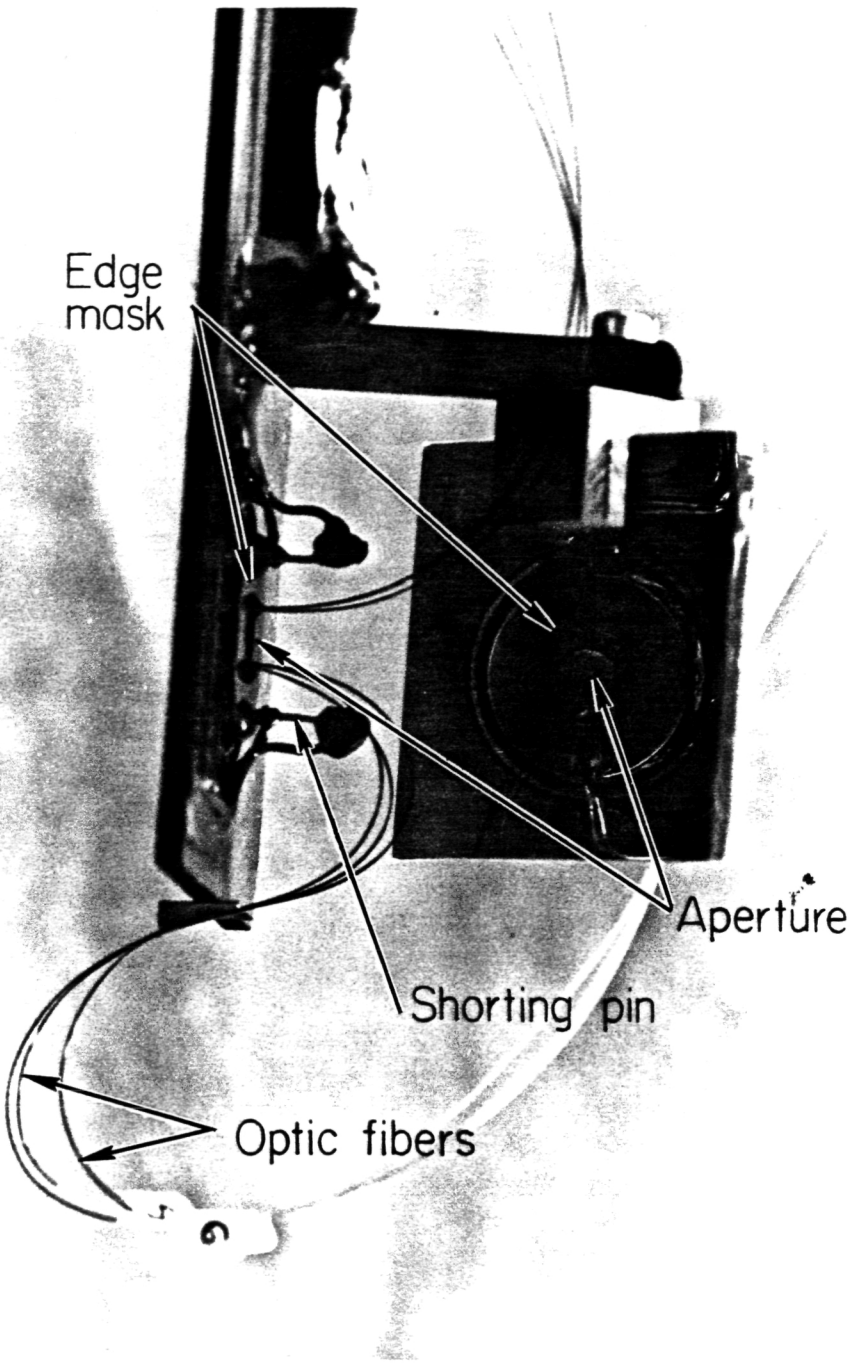

TJA84054SPH

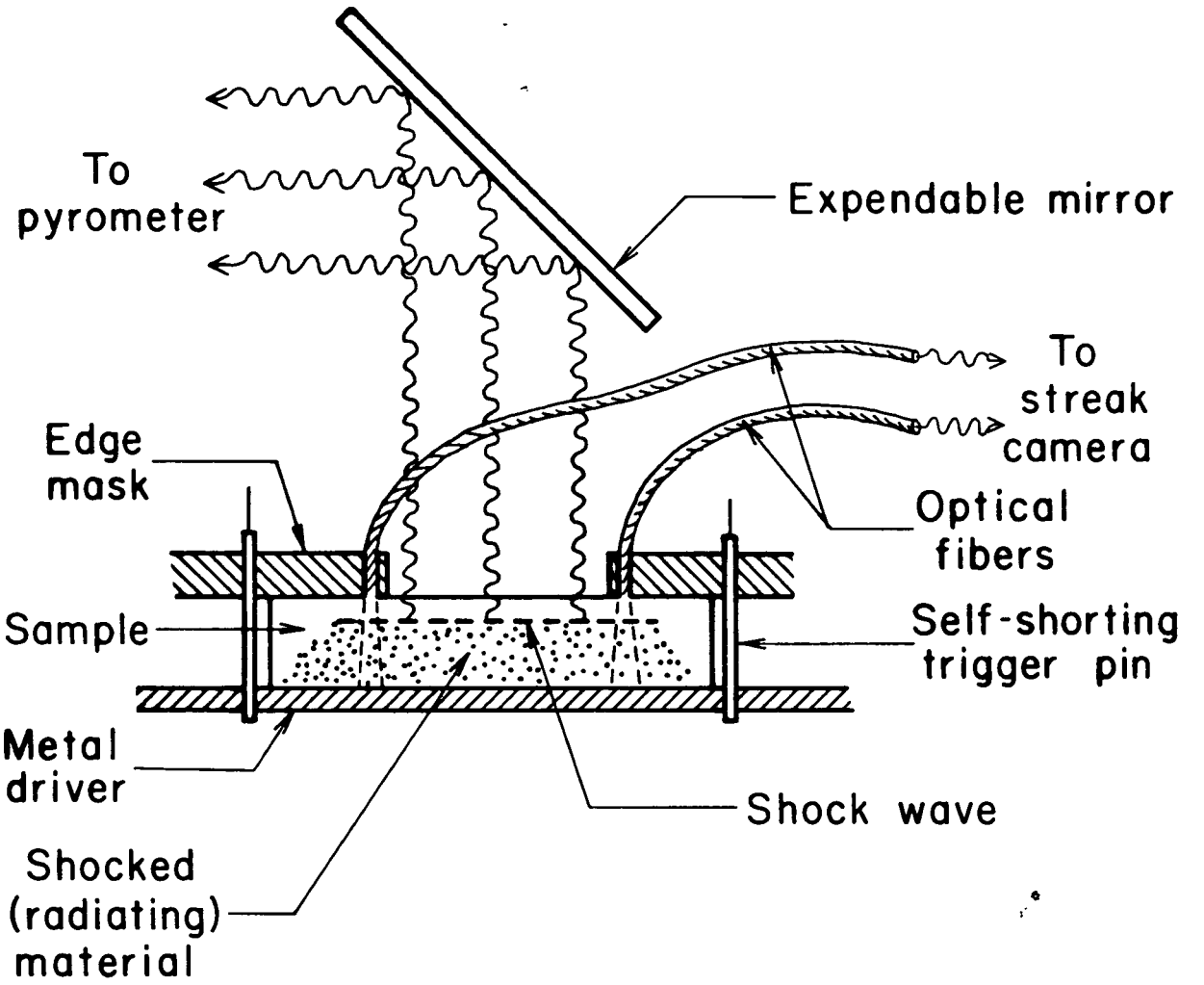

TJA83126SFD

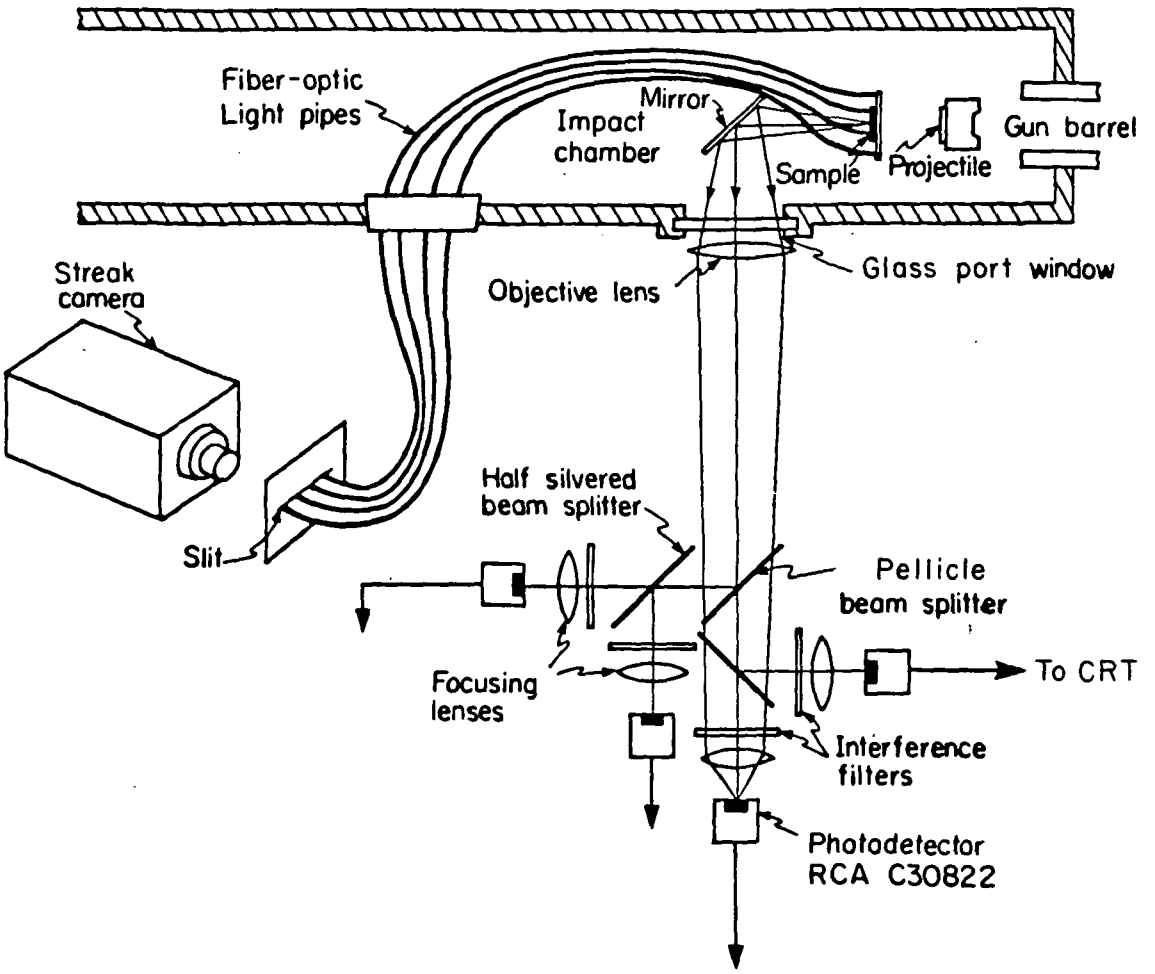
Fiber-optic
Light pipes
Mirror
Impact
chamber
Sample
Projectile
Gun barrel
Streak
camera
Objective lens
Glass port window
Half silvered
beam splitter
Slit
Pellicle
beam splitter
To CRT
Focusing
lenses
Interference
filters
Photodetector
RCA C30822

TJA84055SP

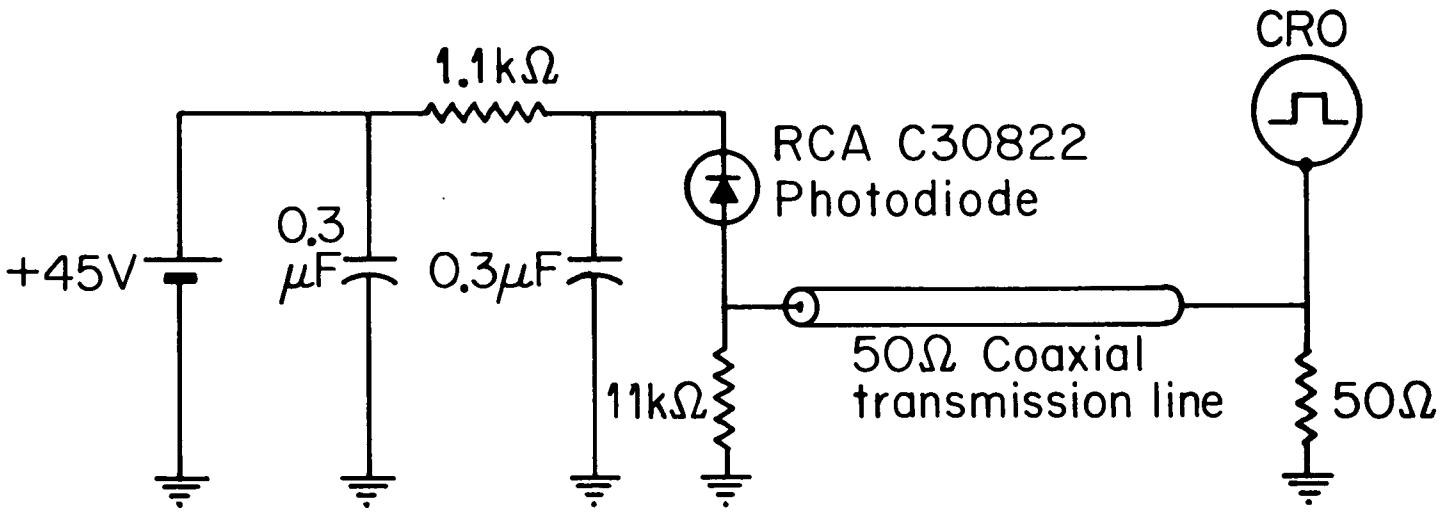

TJA84056SFD

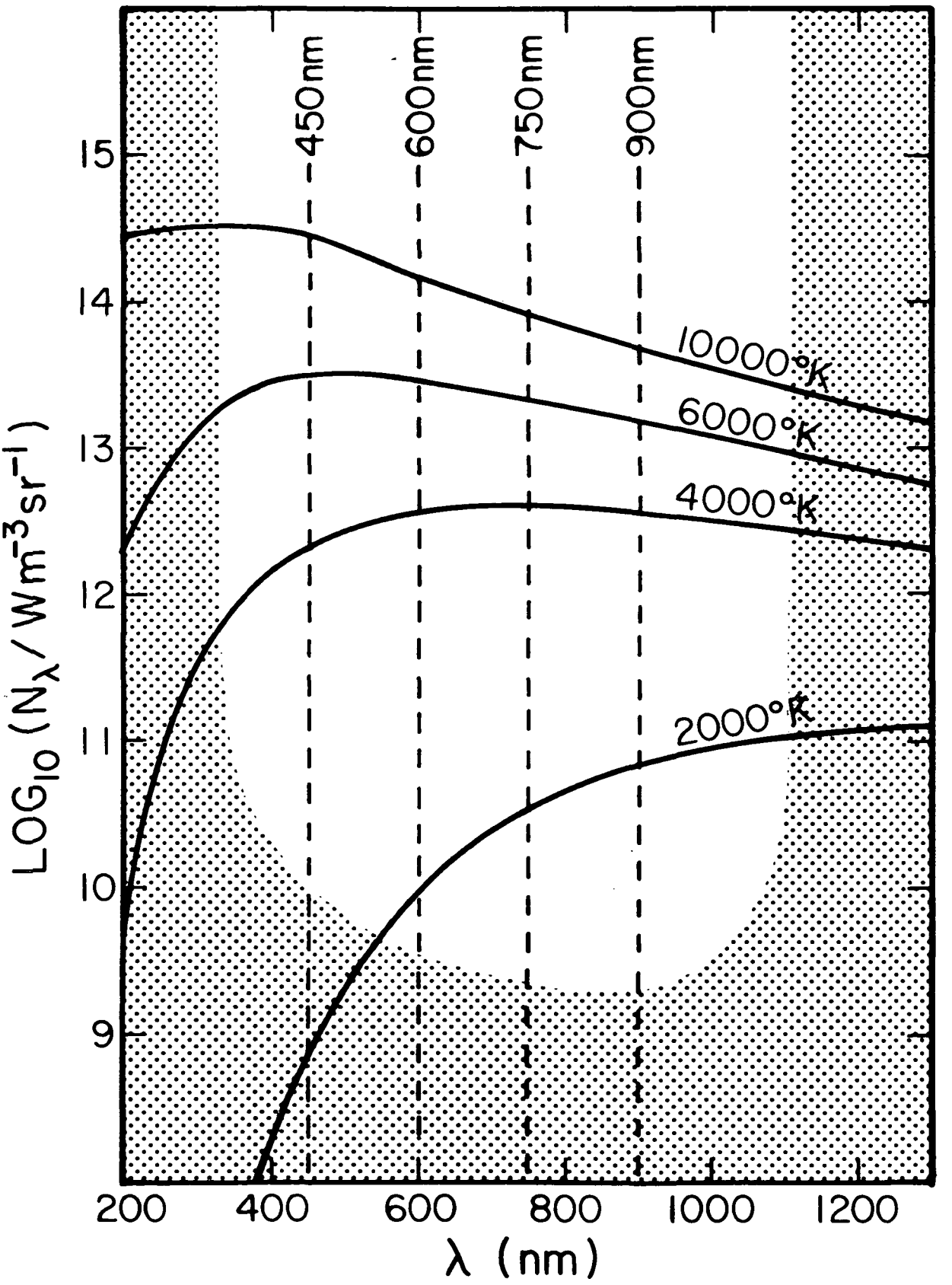

5

TJA84057SFD

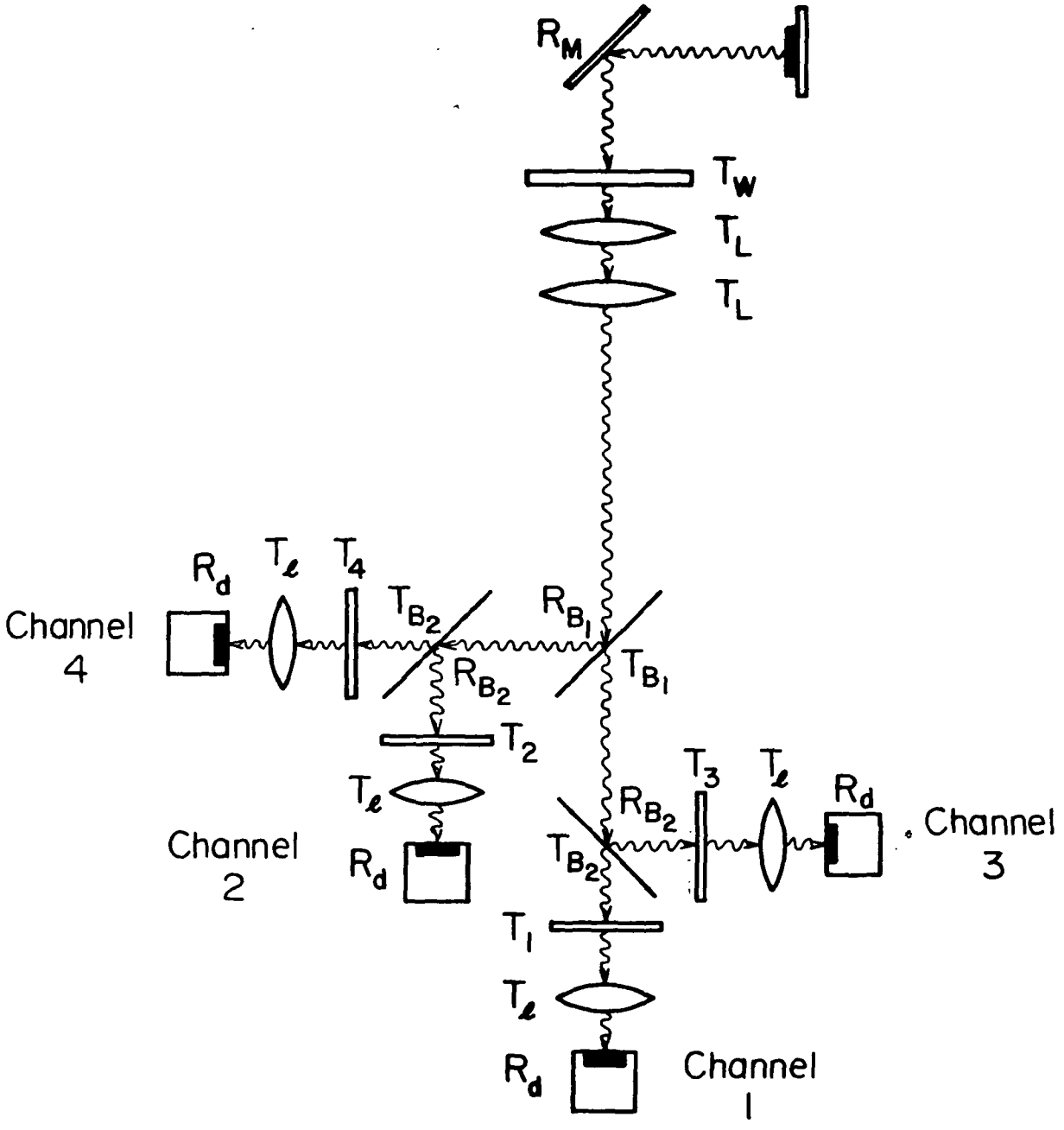

TJA84058SFD

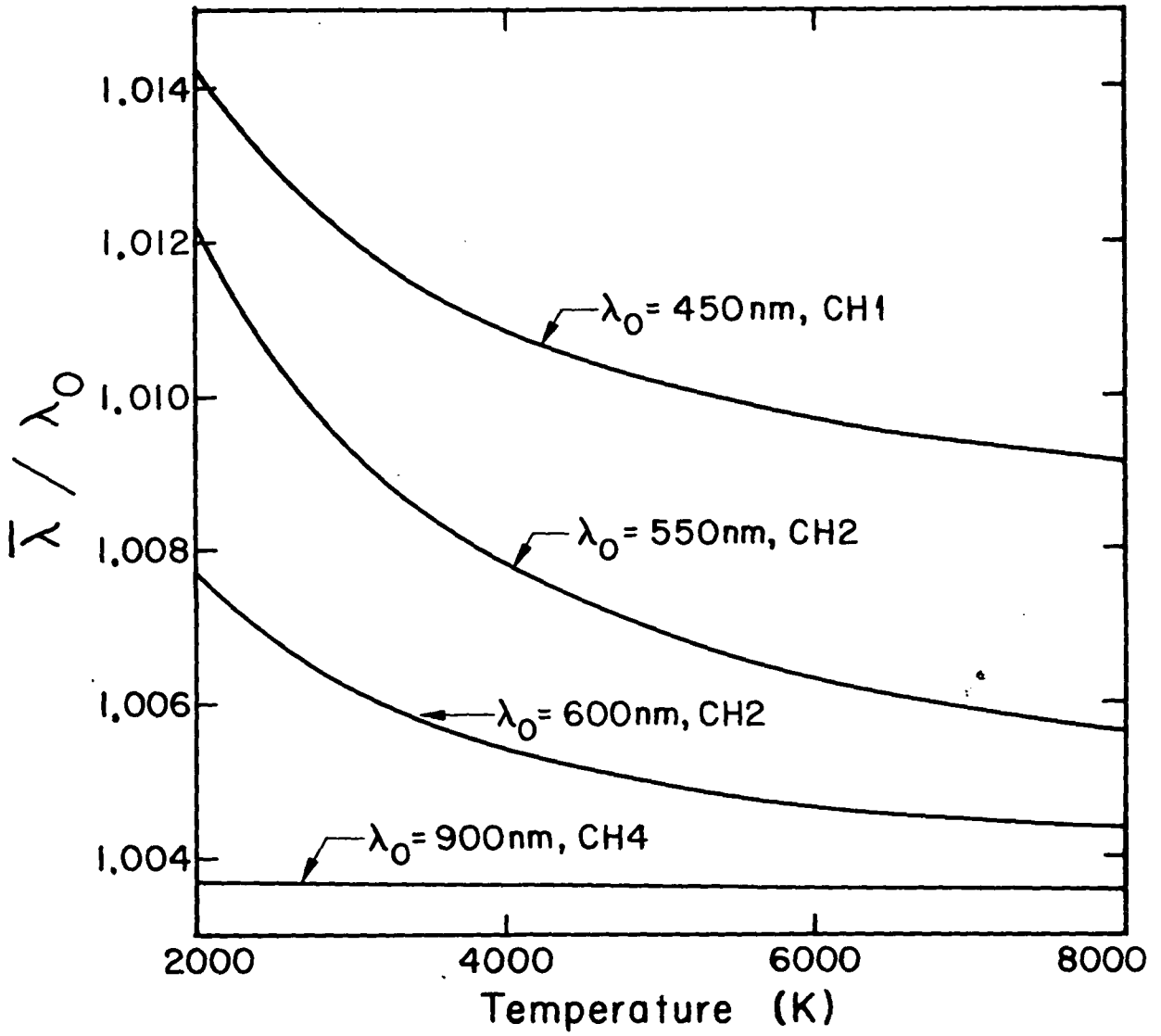

TJA84059SFD

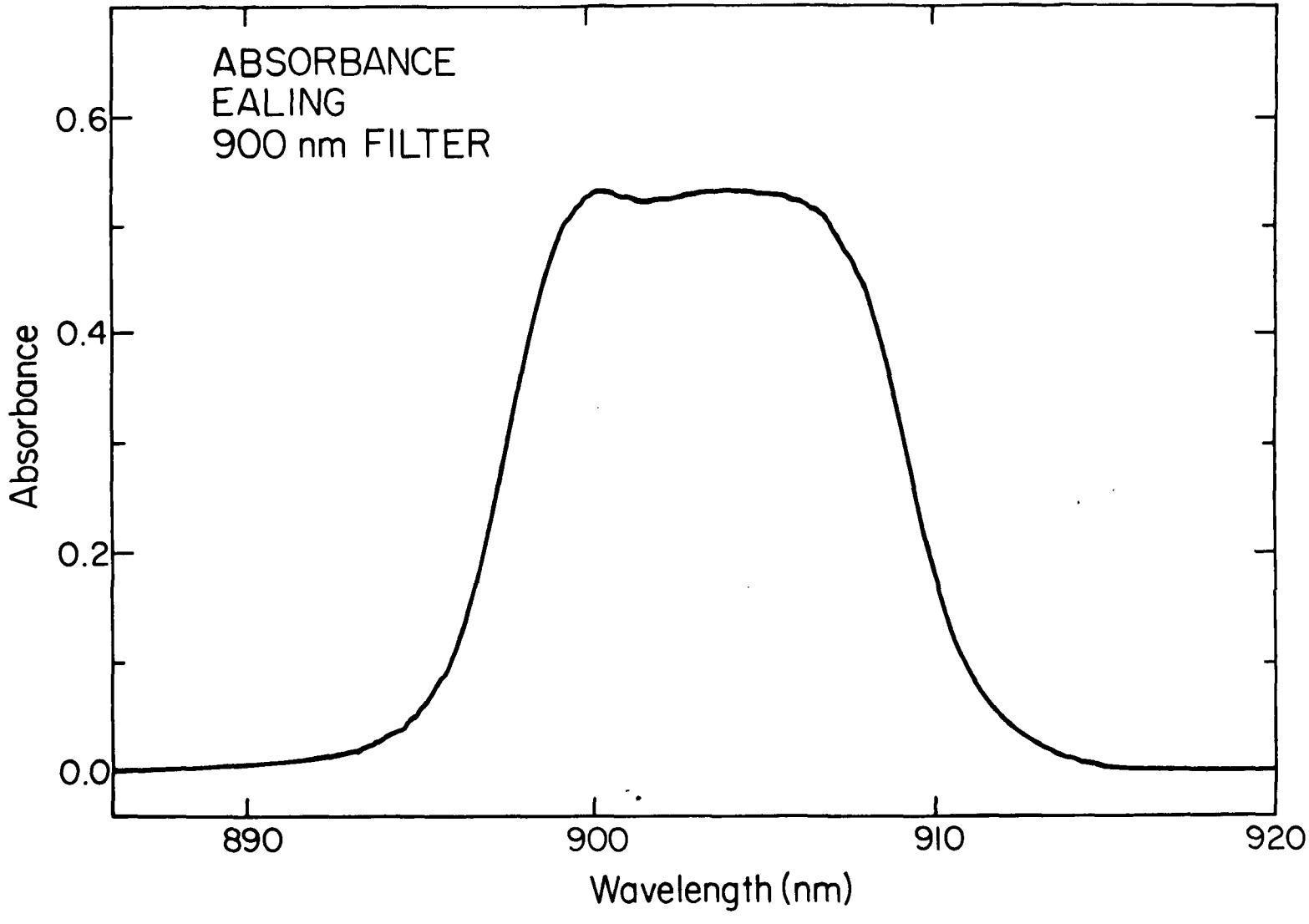
ABSORBANCE
EALING
900 nm FILTER
Absorbance
0.6
0.4
0.2
0.0
890
900
910
920
Wavelength (nm)

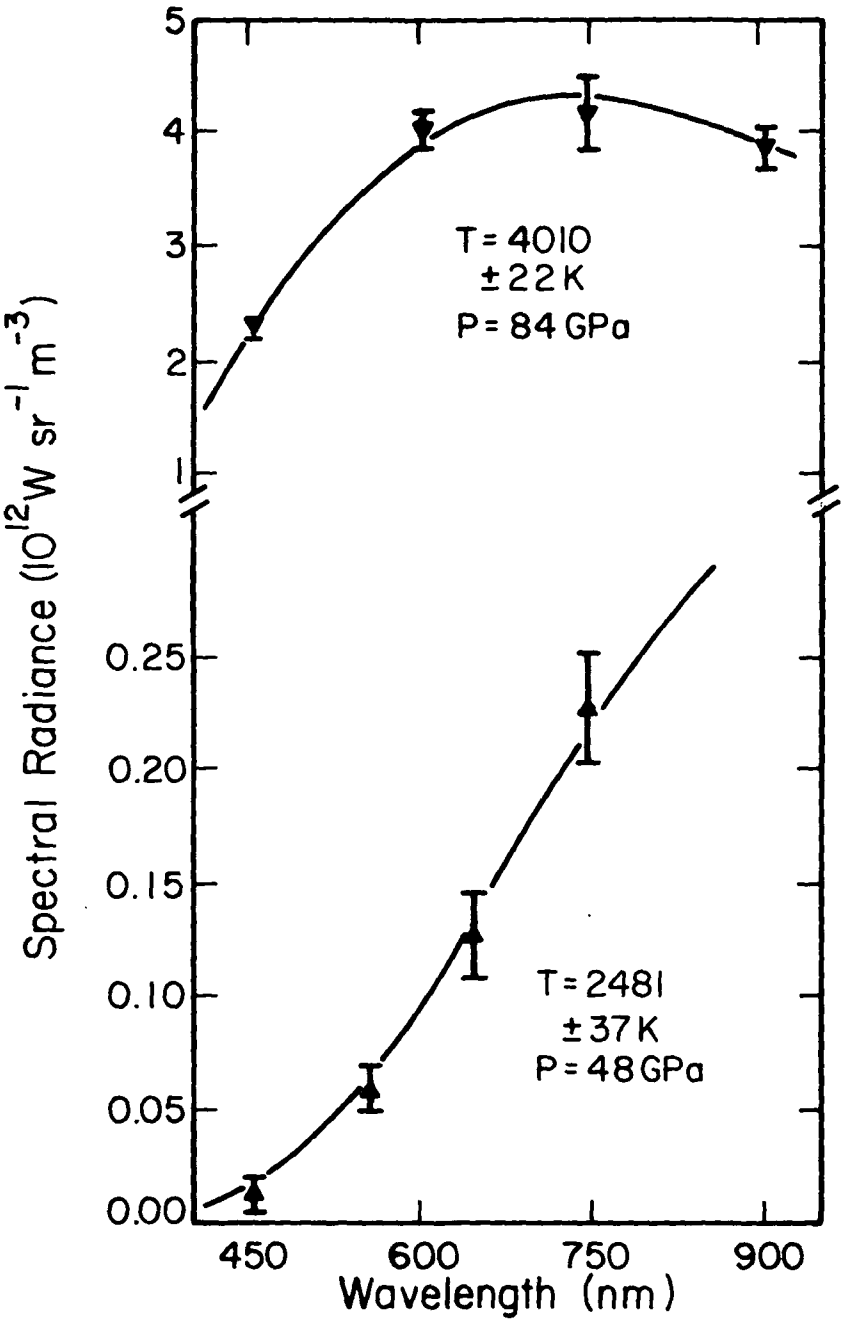

TJA84061SFD